Zwitterionic Polymer Brushes and Core-Shell Particles Based thereon for Control of Biofouling

Fabian Kopsch, Astrid Drechsler, Martina Priebs, Anja Caspari, Anett Müller, Sarah Lentz, Jens Friedrichs, and Alla Synytska*

Dedicated to Brigitte Voit on the occasion of her 60th birthday

Biofilm formation on material surfaces – biofouling – has a significant economic impact on a wide range of applications and industries. There is a huge need for the prevention of undesired interactions of coatings with proteins, cells, and bacteria in biomaterials, biosensors, and other applications. In this work, the preparation and characterization as well as the comparison of bio-fouling properties of surfaces based on planar zwitterionic polymer brushes made of poly(sulfobetaine methacrylate) P(SBMA-3), poly(carboxybetaine methacrylate) P(CBMA-2), or poly(2-methacryloyloxyethyl phosphorylcholine) P(MPC-2) are reported. Since polymer brushes on planar surfaces have disadvantages with regard to layer stability, industrial scaling, and the coating of complex geometries, nano- and microstructured coatings based on polymer-functionalized core-shell particles are subsequently produced. It is found that coatings based on poly(phosphorylcholine) P(MPC-2) modified particles with a diameter of 100 nm have the lowest bioadhesion compared to other particle sizes and chemical compositions. The particle-based coatings developed can pave the way for developing scalable anti-fouling coatings in the future.

F. Kopsch, A. Drechsler, M. Priebs, A. Caspari, A. Müller, J. Friedrichs, A. Synytska
Department of Polymer Interfaces
Leibniz Institute of Polymer Research Dresden
Hohe Str. 6, 01069 Dresden, Germany
E-mail: alla.synytska@uni-bayreuth.de

F. Kopsch, A. Synytska
Chair of Physical Chemistry of Polymeric Materials
Technical University Dresden
01062 Dresden, Germany

S. Lentz, A. Synytska
Functional Polymer Interfaces Group, Bayerisches Polymerinstitut (BPI)
Universität Bayreuth
Universitätsstraße 30, 95447 Bayreuth, Germany

J. Friedrichs
Institute of Biofunctional Polymer Materials, Department of Biointerfaces
Leibniz Institute of Polymer Research Dresden
Hohe Str. 6, 01069 Dresden, Germany

The ORCID identification number(s) for the author(s) of this article can be found under https://doi.org/10.1002/macp.202200454

1. Introduction

Biofouling – the undesired accumulation of proteins, cells, bacteria, and micro- or macroorganisms on surfaces – is encountered in many areas of daily life, such as biomedical devices or implants, carriers for drug delivery, catheters, vascular stents, biosensors, medical equipment, or marine ships.[1–3] Biofouling is a process that proceeds in several phases. In the first step, proteins adsorb on the surface, creating a foundation for the subsequent attachment of bacteria and other organisms.[3] While the first step, the build-up of a protein layer or corona (in the case of particulate systems), is already completed within seconds or minutes, the second step, the primary attachment of bacteria and organisms, usually takes between minutes and several hours. Subsequently, the adhering organisms multiply on the surface and form a biofilm, which is often difficult to dislodge or can only be removed by applying very harsh treatment conditions.[1] Consequently, the research focus in recent years has been on the design and synthesis of bioinert and biocompatible antifouling materials that minimize the initial adhesion of bacteria in particular.[3]

Numerous approaches for antifouling surfaces with different chemical or structural properties and different surface topographies have already been elaborated, including, for example, surfaces based on hydrophilic and/or zwitterionic polymers.[3] Several requirements were identified that antifouling materials should meet: they should reduce the initial, non-specific adsorption of proteins, cells, and bacteria, be polar and electrically neutral, and be hydrogen bond acceptors but not hydrogen bond donors. In addition, most of the proposed materials were hydrated zwitterionic cosmotropes, that is, materials that are able to stabilize protein structures in an aqueous environment.[4]

The gold standard for an antifouling material to date has been the hydrophilic polymer polyethylene glycol (PEG). Since the pioneering work of Prime and Whitesides,[5] who demonstrated the protein-repelling effect of oligo ethylene glycol, this molecule has formed the basis of modern antifouling coatings. For example, the adhesion of *Escherichia coli, Pseudomonas aeruginosa*, and *Staphylococcus aureus* to silicon wafers has been significantly reduced by functional coatings based on PEG polymer brushes.[6] PEG-based biopassive polymers are promising as they form a

hydration layer near the surface that acts as a physical barrier and thereby prevents direct contact between the surface and proteins, cells, or bacteria.[2,7] A disadvantage of these materials, which often makes their long-term use impractical, is their lack of oxidation stability and, thus their susceptibility to degradation.[2–8]

In contrast, another class of polymers, the amphoteric and zwitterionic polymers, has recently moved into the focus of research.[4–9] These polymers have the same number of positive and negative charges in their polymer chains and form (in the form of polymer brushes, which are monolayers of polymer chains chemically attached by one end to a substrate[10]) a denser hydration layer due to electrostatic interactions, which can prevent the adsorption of biomolecules more effectively, even compared to purely hydrophilic polymers such as PEG.[2–11] Zwitterionic polymers show a higher degree of swelling in aqueous salt solutions, improving their antifouling properties and setting them apart from previously used compounds such as PEG. Especially in the development of biomaterials used in aqueous solutions with high ionic strength (e.g. catheters), coatings based on zwitterionic molecules offer opportunities for new developments. Building on Ishihara et al.[12] who demonstrated in 1991 that using zwitterionic polymers reduces the adsorption of human blood plasma proteins, this class of molecules is of great interest in this field. In particular, poly(sulfobetaines) (SB),[3–13] poly(carboxybetaines) (CB),[14] and poly(phosphorylcholines) (PC)[2–15] have been tested in numerous studies for their effectiveness in reducing biofouling. When comparing theoretical simulations of CB and SB, the sulfonate group of SB was found to coordinate more water molecules, whereas CB-coordinated water molecules had a sharper spatial distribution and longer residence times in the hydration shell.[11] It is assumed that the different hydration capacities influence the antifouling properties of these zwitterionic molecules.[11] Another advantage of using zwitterionic polymers is their increased stability in aqueous, acidic, or alkaline media. For example, SB was stored for one year in 1 M NaOH and in 1 M HCl without being degraded.[4] The hydrolytic stability results from the shielding of the polymer backbone by the steric hindrance of the ester and amine groups, which qualifies zwitterionic polymers as promising candidates for durable antifouling coatings.[4]

Planar surfaces based on zwitterionic polymers or polymer brushes have mostly been investigated on a laboratory scale as model systems. These types of coatings have certain disadvantages due to their low robustness and lack of practicability towards covering large-area substrates when it comes to their use on an industrial scale.

Coatings based on core-shell particles could offer an alternative platform for avoiding these disadvantages. Their inorganic core provides the necessary surface robustness of corresponding coatings, while the organic shell enables the chemical modification of the surface. Moreover, particles grant access to microscale-structured polymer brush scaffolds. Particle-based building blocks provide a large surface area and can be synthesized on large scale in a controlled way. In addition, the particles can be applied to large and topographically complex surfaces using industrially scalable processes (e.g. spray coating). Also, the choice of core size can change the microtopography of the coatings produced and thus vary a surface parameter that has been shown to influence the adhesion of bacteria. Molino

et al. demonstrated in several publications the potential of antifouling coatings based on silica nanoparticles with zwitterionic shells.[11–16] The silica core included diameters from 7 to 75 nm and SB- or CB-containing shells. By assembling these particles into multilayer coatings, *E. coli* adhesion was reduced by up to 94 %. However, the surface root mean square roughness of these nanoparticle-based coatings was still lower than 20 nm due to the small particle size.

In this work, we report on the fabrication of flat and micro-structured surfaces made of zwitterionic polymer brushes as well as core-shell particles based on them (**Figure 1**) and investigate their surface-specific bio(anti)fouling properties. For this, three families of zwitterionic polymer brushes based on poly(sulfobetaines), poly(carboxybetaines), and poly(phosphorylcholines) are synthesized on planar and particle surfaces. We systematically adjust surface morphology and roughness by varying the particle size between 100, 400, and 800 nm. We address the question of transferability of the results received from topographically plain and flat to structured and curved substrates as well as the appropriate radius of curvature according to the anti-bioadhesive properties of gram-negative *E. coli* bacteria.

Core-shell particles with grafted PEGMA served as positive controls in all experiments. Physical properties of the developed layers (surface charge at different pH, ionic strength and morphology, roughness) were characterized and the ability to reduce bacterial adhesion was assessed.

2. Results and Discussion

2.1. Flat Zwitterionic Polymer Brush Coatings

Zwitterionic polymer brushes – P(SBMA-3), P(CBMA-2), and P(MPC-2) – as well as uncharged poly(poly(ethylene glycol) methacrylate) P(EGMA) as a reference system were synthesized on planar SiO₂ substrates using a grafting-from approach. Briefly, amino groups introduced onto the SiO_2 surface by 3-(aminopropyl)triethoxysilane (APTES) treatment were used for the subsequent coupling of the ATRP-initiator α-bromoisobutyryl bromide.[17] Polymer brushes were formed on the initiator-modified surfaces from zwitterionic monomers by activators regenerated by electron transfer atom transfer radical polymerization (ARGET-ATRP) (Figure 1).[18,19] The thickness in dry state and the wettability of the synthesized brushes were characterized using null ellipsometry and dynamic water contact angle measurements (**Table 1**).

Null ellipsometry yielded brush thicknesses exceeding 10 nm for all systems in the dry state, ensuring complete substrate coverage. All polymer-modified surfaces are hydrophilic, with advancing water contact angles of less than 40°. The water contact angles for P(EGMA), P(SBMA-3), and P(MPC-2) brushes closely match published data.[20–22] The water contact angle on P(CBMA-2) was slightly higher than previously reported;[23] the deviation is explained by the short hybridization time of the P(CBMA-2) brushes during the measurement.[19]

Streaming current measurements were performed to determine the apparent zeta potential of the brushes (Figure S1, Supporting Information). The variation of the curves, especially the shift of the isoelectric point (IEP; zero crossing of the zeta
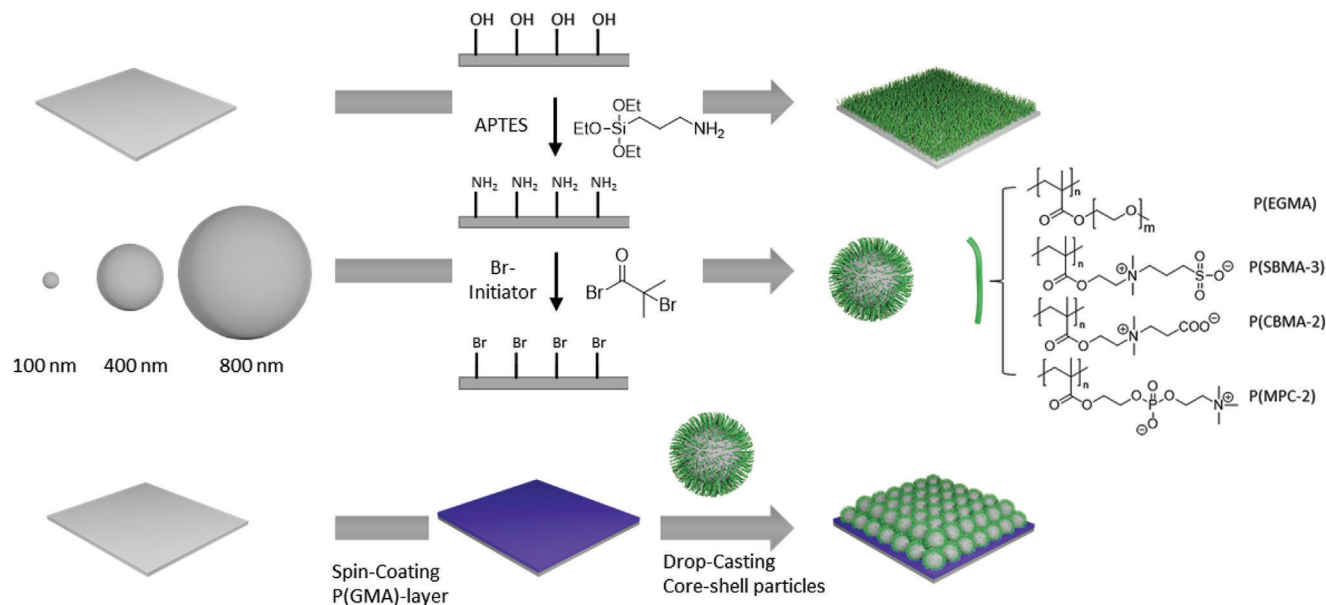
ADVANCED
SCIENCE NEWS
www.advancedsciencenews.com

[M]acro-
molecular
Chemistry and Physics
www.mcp-journal.de

Figure 1. Native flat silicon wafers and spherical SiO$_2$ particles (100, 400, and 800 nm) were modified with APTES and Br-initiator. Performing SI-ATRP grafting-from polymerization, the surfaces were modified with zwitterionic polymer brushes, namely poly(sulfobetaine methacrylate) P(SBMA-3), poly(carboxybetaine methacrylate) P(CBMA-2), and poly(2-methacryloyloxyethyl phosphorylcholine) P(MPC-2). Finally, the core-shell particles were processed into multilayer particle coatings.

Table 1. Dry thickness and advancing/receding water contact angle (CA) of polymer brushes grafted on APTES-modified silicon surfaces.

Polymer	Brush thickness [nm]	Water contact angles and SD [°]	
		Advancing CA	Receding CA
P(EGMA)	54.1 ± 3.6	34.8 ± 0.2	14.6 ± 0.3
P(SBMA-3)	14.2 ± 1.6	13.2 ± 0	< 10
P(CBMA-2)	24.6 ± 3.9	27.5 ± 0.1	< 10
P(MPC-2)	11.2 ± 1.6	< 10	< 10

potential) proves the successful modification. For plain SiO$_2$ the IEP is around pH 2.5 as a result of the acidic behavior of its hydroxyl groups. After the deposition of APTES, the IEP shifts to pH 7 due to the basic amino groups. The different curve shape and IEP measured for the polymer brushes reflect their electric properties and swelling behavior. P(EGMA) and P(MPC-2) brushes exhibit very low absolute values of the zeta potential, which indicates a high-water content, that is, strong swelling. The plateau values decrease from -6 mV for P(MPC-2) via -17 mV for P(EGMA)[24] to −30 mV for P(SBMA-3). The IEP is around pH 4 for the three brushes. This is a typical feature of surfaces with low or nearly balanced intrinsic charges. On the contrary, P(CBMA-2) has an IEP at pH 6 and maximum plateau values around +40 mV in the acidic range and −40 mV in the alkaline range. This shows that the surface of this brush is dominated by alkaline functionalities. It should be noted that the data for P(EGMA) was taken from an earlier study[24] and measured under different measuring conditions. This might affect the absolute values slightly but the shape of the curve and the IEP should remain similar, allowing comparison with the zwitterionic polymers.

The morphology and swelling behavior of the brushes were studied by AFM imaging and force measurements. As an example, **Figure 2** presents height images of the P(SBMA-3) brush and force-distance curves measured between this brush and a sharp silicon tip. The AFM images and force-distance curves of all brushes are shown in the Supporting Information (Figures S2 and S3, Supporting Information).

The AFM images in dry state show very smooth layers with a root mean square (RMS) roughness of less than 0.5 nm. In electrolyte solutions, the brushes were swollen, as can be seen from the high decay length of the force-distance curves (Figure 2C). The swelling increases the waviness of the surface slightly, leading to RMS values of about 1 nm (for an imaging force of 1 nN). This value depends more on the imaging force than on the composition and concentration of the solution. The other brushes exhibited similar features except for a much stronger swelling of the P(EGMA) brush resulting from the much higher dry thickness (see Table 1). From the force-distance curves (Figures S2 and S3, Supporting Information), the swollen brush thickness was derived. For P(SBMA-3), it is 40–50 nm for most solutions. A slightly stronger swelling was observed in 750 mM NaCl (≈60 nm) (Figure 2C). The P(CBMA-2) brush had a thickness of 30–40 nm in all solutions. For P(MPC-2), it varied between 50 and 60 nm. On the contrary, the uncharged P(EGMA) brush exhibited a thickness of 140–160 nm, independent of the electrolyte solution.

Afterward, the protein adsorption behavior onto the planar zwitterionic polymer brushes compared to a positive (P(EGMA)) and negative control (gold substrate) was quantified by quartz crystal microbalance using the model protein bovine serum albumin (BSA) (**Figure 3**A). Compared to the negative control, all polymer brushes showed significantly lower BSA adsorption, with P(SBMA-3) and P(CBMA-2) achieving comparable or even
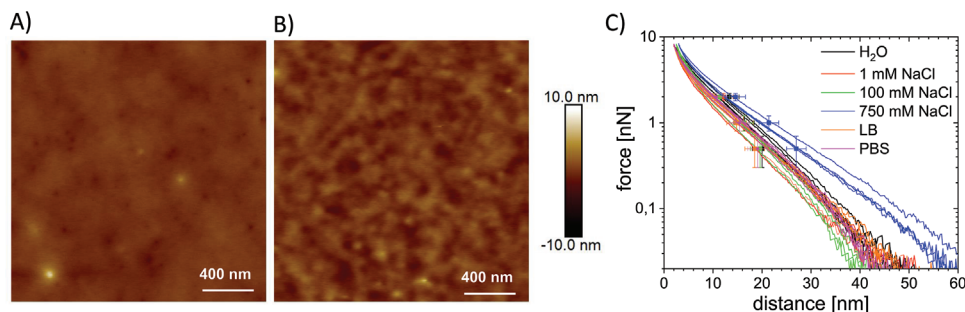
**ADVANCED
SCIENCE NEWS**

www.advancedsciencenews.com

⌈M⌉ **acro-
molecular**
Chemistry and **Physics**

www.mcp-journal.de

Figure 2. AFM investigation of P(SBMA-3) brushes on a flat substrate: A) height image in air, B) height image in PBS buffer, and C) force-distance relation between AFM tip and brush in various solutions. The crosses mark the film thickness obtained by an AFM scratch test with different loads (0.5, 1, and 2 nN).
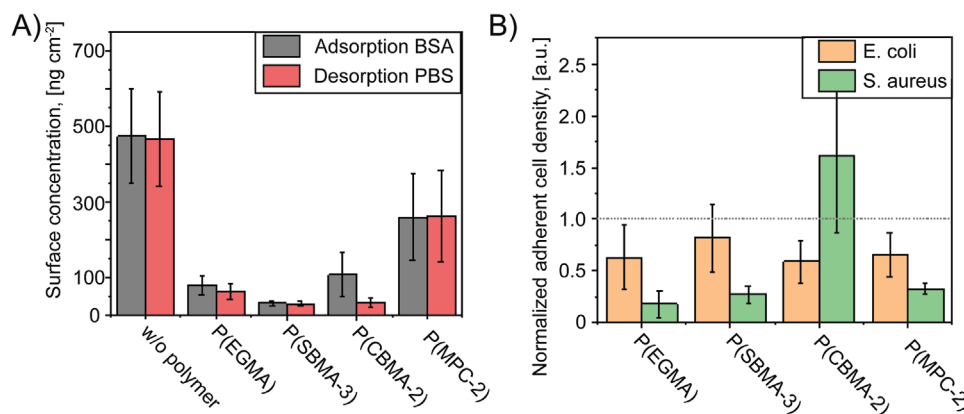

Figure 3. A) Adsorbed amount of bovine serum albumin on polymer-modified surfaces, determined by quartz crystal microbalance measurements. The protein solution was adsorbed to the samples for 1 h and subsequently subjected to a desorption regime for 30 min with PBS. B) Normalized adherent cell densities of *Staphylococcus aureus* (*S. aureus*) and *Escherichia coli* (*E. coli*) on polymer-modified surfaces. Data are normalized by the average adherent cell density on an RCA-cleaned silica substrate. Graphs show the mean ± SD. Data were obtained from at least three independent experiments.

lower values than the positive control P(EGMA). Only P(MPC-2) brushes adsorbed more BSA than P(EGMA).[1–25]

Next, the adhesion of Gram-negative *Escherichia coli* (*E. coli*) and Gram-positive *Staphylococcus areus* (*S. aureus*) bacteria to the polymer brushes was subsequently tested (Figure 3B). *E. coli* adhesion was significantly reduced on the P(CBMA-2) and P(MPC-2) surfaces, comparable to the values of the positive control P(EGMA). Slightly higher *E. coli* adhesion was observed on P(SBMA-3) surfaces. A different trend was found for the adhesion of *S. aureus* to the surfaces tested. P(SBMA-3) and P(MPC-2) brushes reduced bacterial adhesion to the level of P(EGMA), while even more cells adhered to P(CBMA-2) surfaces than to the negative control (silica substrate). The results show that polymer brushes based on zwitterionic polymers have a potential for reducing bioadhesion, mainly comparable to the gold standard P(EGMA). However, the zwitterionic polymer brushes can only be economically produced on a laboratory scale and in low layer thicknesses on flat surfaces. They also have limitations regarding their layer stability.

2.2. Core-Shell Particles

From this perspective, core-shell particles comprising a zwitterionic polymer shell represent an interesting option for prepar-

ing anti-adhesive coatings that can overcome the disadvantages of flat polymer brushes. Particle-based coatings are more wear-resistant and can be processed using various methods such as spray coating, dip coating, spin coating, doctor blading, or drop-casting. Consequently, core-shell particles were synthesized from SiO_2 cores by covering them with uncharged P(EGMA) or zwitterionic polymer brushes P(CBMA-2), P(SBMA-3), and P(MPC-2). The influence of core size, different surface charges, and chemistry on the surface roughness and anti-adhesive properties of the resulting layers was investigated.

2.3. Synthesis and Characterization of Silica-Based Core-Shell Particles

The particle cores were silica-based Stöber particles with diameters of 100, 400, and 800 nm. These SiO_2 particles were modified by attaching first APTES and then ATRP-Br-initiator (Figure 1). On this anchor layer, SI-ATRP grafting-from polymerization was performed to functionalize the SiO_2 surface with a polymeric shell with the polymers previously used for polymer brushes on flat surfaces. The brush-covered particles were analyzed using scanning electron microscopy (SEM) to check the success of the grafting procedure. Thermogravimetric analysis (TGA) was performed to determine the mass fraction of the

**ADVANCED
SCIENCE NEWS**

www.advancedsciencenews.com

[M] acro-
molecular
Chemistry and Physics

www.mcp-journal.de

Table 2. Zwitterionic polymer brush thicknesses on SiO_2 particles obtained from TGA measurements.

Polymer core	P(EGMA) [nm]	P(SBMA-3) [nm]	P(CBMA-2) [nm]	P(MPC-2) [nm]
100 nm SiO_2 particle	28.9	22.6	29.1	5.1
400 nm SiO_2 particle	148.5	64.3	26.1	21.9
800 nm SiO_2 particle	83.9	10.4	17.7	5.3

polymer shell and to estimate the brush thickness. The SEM images show the presence of polymer shells (Figures S4 and S6, Supporting Information) whose thickness varies between the individual samples. TGA allows the quantitative calculation of the dry brush thickness (H) using Equation (1)[26]

$$H = \frac{\frac{R}{3} * m_{polymer} * \rho_{Silica}}{\rho_{Polymer} * (1 - m_{polymer})} \qquad (1)$$

where R is the radius of the particle, ρ the mass density, and $m_{polymer}$ the mass fraction of the polymer obtained using TGA (Figure S7, Supporting Information)

The resulting polymer brush thickness values are summarized in **Table 2**. Significant variations in P(EGMA), P(SBMA-3), and P(MPC-2) shell thickness were observed for different particle diameters, an effect not detected for P(CBMA-2). That behavior can be explained by the presence of inhibitor molecules in the commercial monomers SBMA-3 and MPC-2. In most cases, P(CBMA-2) brushes had the highest and P(MPC-2) the lowest chain length.

2.4. Electrokinetic Measurements

After each step of the particle modification, electrokinetic measurements of particle dispersions were performed to verify the success and quality of these modifications. In **Figure 4** the data for the 400 nm particles are shown as an example; Figure S8, Supporting Information, presents the results for 100 and 800 nm particles. The IEP of all samples are listed in Table S1, Supporting Information. As for the flat brushes, the shape of the zeta potential curves and the IEP proved the success of the modification and reflected the swelling and electric properties of the polymer brush shells. As expected, these properties did not change for particles of different sizes with the same polymer shell. Due to their acidic –OH functionalities, the native SiO_2 particles exhibited a negative potential over a wide pH range (< 2.5–10, Figure 4). As a result of the alkaline amino groups formed during chemisorption of APTES, a positive zeta potential is generated at the particle surface up to the isoelectric point (IEP) at pH 7 (Figure 4). The success of the last pre-modification step – the coupling of the bromine initiator to the APTES-modified SiO_2 surface – is demonstrated by a shift back to about 3.5 as expected for the primarily uncharged initiator. These results correspond well to electrokinetic measurements published earlier.[27] From the IEP of the polymer-grafted particles, their acid-base properties can be derived. The lowest IEP (< 2.3), that is, acidic behavior, was observed for P(SBMA-3) modifications which are consequently negatively charged during the bacterial adhesion experiments at pH
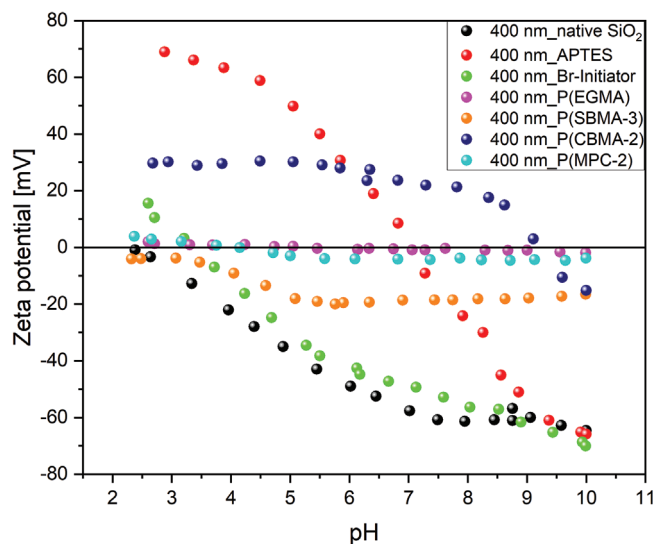

Figure 4. pH-dependent zeta potential of native, APTES-, and Br-initiator-modified 400 nm SiO_2 particles and core-shell particles covered with uncharged P(EGMA) or zwitterionic P(SBMA-3), P(CBMA-2), and P(MPC-2) brushes.

~ 7 (Figure 8). An IEP of 4.2 was determined for the P(MPC-2) polymer brushes. The absolute values of the zeta potential are below 10 mV over the entire pH range, which can be an effect of low charge separation of the functional groups but mainly shows the swelling of the polymer chains. The same behavior can be observed for the primarily uncharged P(EGMA) coated particles. In contrast to the somewhat acidic or amphoteric behavior of most zwitterionic brushes, particles modified with P(CBMA-2) brushes had an IEP > 9, indicating the predominance of alkaline groups. Therefore, the surface is positively charged during the bacterial adhesion experiments at pH ≈ 7. The observed differences in the acid-base properties of the zwitterionic polymers are in good agreement with the previously published results from other working groups. For example, Neoh et al.[28] demonstrated the same acidic behavior of P(SBMA-3) brushes on bare silicon substrates. Furthermore, the results of Teramura et al.[29] and Gu et al.[30] showed that the zwitterionic P(MPC-2) and CBMA-2 brushes have almost the same zeta potential over a wide pH range.

2.5. Core-Shell Particle Coatings

After successfully preparing and characterizing the core-shell particles, particle-based coatings were produced. As an adhesion promoter, the hydrophobic poly(glycidyl methacrylate) P(GMA) was spin-coated onto silica wafers in a ≈100 nm thick layer.[27] The core-shell particles were then drop-casted onto the viscous P(GMA) layer and partially sank into it (**Figure 5**). Subsequently, a thermal treatment cross-linked the P(GMA) base layer fixing the particles to the surface. During this process, particle multilayers were formed in which particle layers not in contact with P(GMA) interacted with the bound base particle layer via van-der-Waals or electrostatic forces. These coatings were imaged by AFM in dry state.
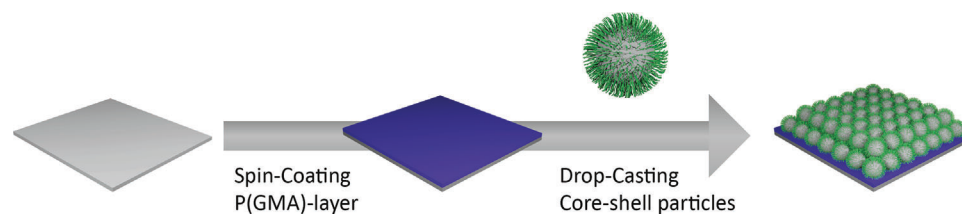
Figure 5. Scheme of the preparation of multilayer particle-based coatings. A cleaned silicon wafer was spin-coated with P(GMA) as a bonding agent. The core-shell particles were immobilized using a drop-casting method to obtain a multilayer particle coating.
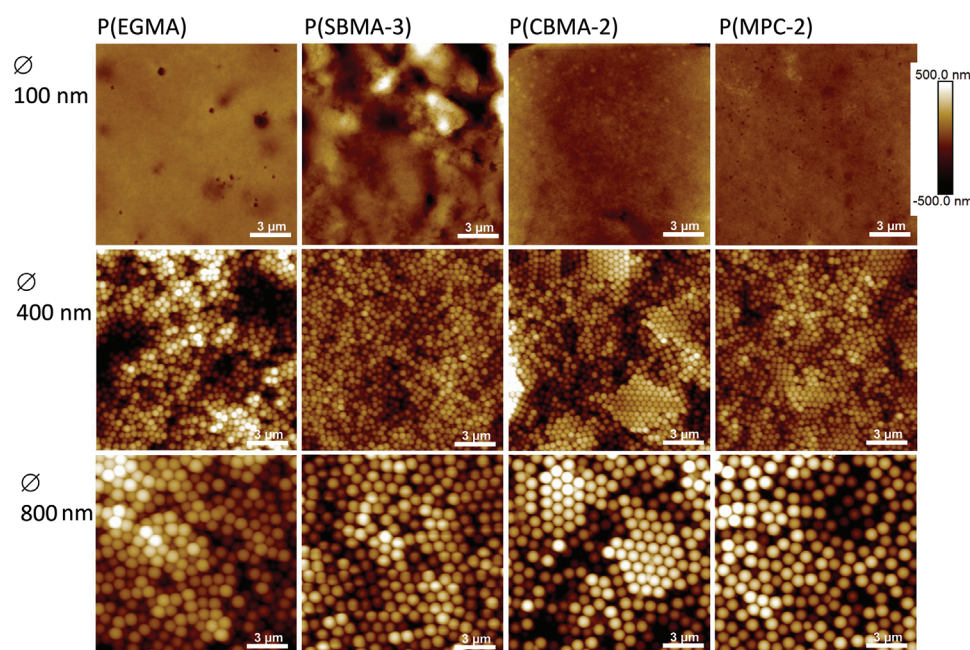

Figure 6. AFM images of coatings made of core-shell particles with SiO_2 cores (diameter 100, 400, and 800 nm) and P(EGMA), P(SBMA-3), P(CBMA-2), and P(MPC-2) shells.

Figure 6 compares the height images of coatings prepared with core-shell particles of 100, 400, and 800 nm diameter covered with P(EGMA) and zwitterionic polymer brushes. For better comparison, the same height scale is used for all images. Additional images of the 100 nm particle films taken with higher magnification can be seen in Figure S9, Supporting Information.

With most particle coatings, relatively uniform layers were obtained. An exception is a layer of P(SBMA-3)-grafted 100 nm particles that have a higher waviness due to an uneven coating of the substrate. The images in Figure S9, Supporting Information, show that on a length scale of a few micrometers, all 100 nm particle layers are smooth arrangements of the core-shell particles. With increasing particle size the topography becomes more dominated by the particle shape. In some layers made of P(CBMA-2) and P(MPC-2) coated SiO_2 particles, small areas of close sphere packings were observed (Figure 6). Obviously, the interaction between the zwitterionic polymers favors self-organization to a certain degree.

The AFM images were analyzed with regard to two essential morphology parameters – the root mean square (RMS) roughness and the developed interfacial area ratio (Sdr). To include a comparable number of particles despite their different size, the calculations were performed for square areas with a side length of approximately 20 times the particle diameter. They, therefore, yield an average roughness of the particle layer, not the surface roughness of the single particles. It is assumed that the latter is comparable to that of the flat brushes with an RMS roughness in the order of 1 nm.

Increasing the particle size naturally increases the RMS roughness of the particle layer (**Figure 7**). With 100 nm particles, it is in the order of 20 nm. These RMS values are comparable to those of core-shell particle coatings fabricated by Molino et al. with 75 nm particles. They showed an RMS roughness of about 17 nm.[11–16] For P(SBMA-3), it is a bit higher due to the uneven coating. The RMS roughness of coatings based on 400 nm core-shell particles is increased to 100–200 nm, and the SiO_2-P(SBMA 3) and SiO_2-P(MPC-2) layers are smoother than SiO_2-P(CBMA-2). The higher RMS roughness of the SiO_2-P(CBMA-2) particle coating is due to forming sphere clusters with larger voids. Using 800 nm core-shell particles as a coating base increased the RMS value to about 250 nm.

The Sdr value is a measure of the surface increase by 3D structuring compared to the projected (2D) surface. It might thus play an important role in bacterial adhesion. The Sdr values of the
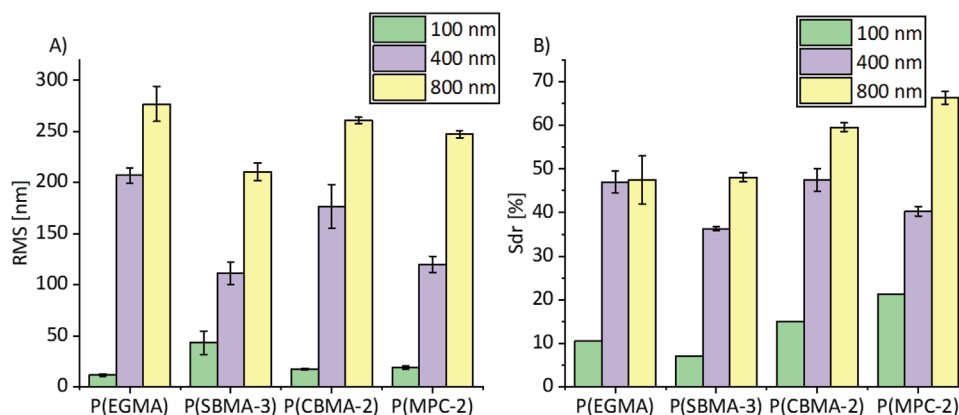
**ADVANCED
SCIENCE NEWS**

www.advancedsciencenews.com

**Macro-
molecular
Chemistry and Physics**

www.mcp-journal.de

Figure 7. A) RMS roughness and B) Sdr values of coatings made of core-shell particles with SiO_2 cores (diameter 100, 400, and 800 nm) and P(EGMA), P(SBMA-3), P(CBMA-2), and P(MPC-2) shells.
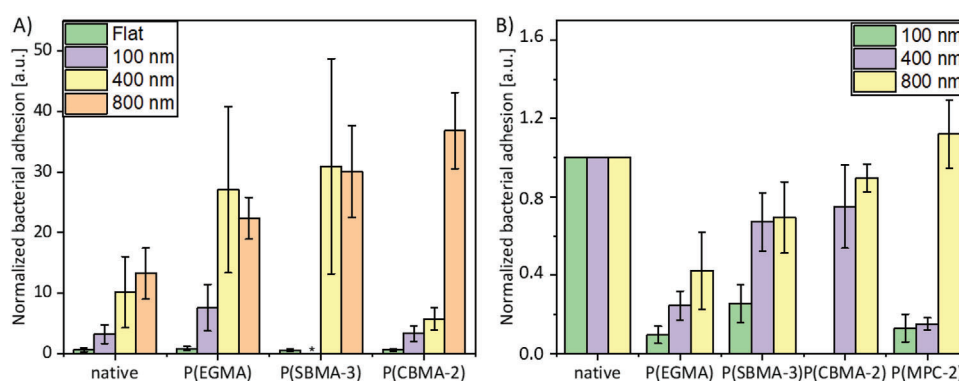

Figure 8. Normalized adherent *E. coli* cell density on particle-based surfaces. Data are normalized to A) the average adherent cell density on an RCA-cleaned silica substrate or to B) the non-polymer modified particle-based surface of the respective particle size. Graphs show the mean value ± SD. Data were obtained from at least three independent experiments.

examined surfaces show the same trend as the RMS roughness but are less sensitive to surface irregularities. The Sdr increases steadily from the flat model systems with values of about 1% to 10–20% for the 100 nm core-shell particle coatings, 30–40% for the 400 nm particle coatings, and 40–65% for the 800 nm core-shell particle coatings. Theoretically, the Sdr of dense sphere packings should be independent of the sphere diameter. In practice, however, the sphere packings are neither dense nor ideal, and voids between the larger particles are more easily accessible to the AFM tip leading to higher values. They might be relevant anyway since the larger voids are not only better accessible for the AFM measurement but also the adhesion of bacteria that are in the same order of magnitude as the apex of the AFM tip.

2.6. Bacterial Adhesion Assay

The anti-bioadhesive properties of the particle-based surfaces were investigated in bacterial adhesion experiments with *E. coli* (**Figure 8**). The main focus was to explore the effect of the surface roughness (depending on the particle sizes used) and the contribution of the different polymer coatings of the particles. As a reference, either flat (non-particle-based) polymer brushes

(Figure 8A) or curved particle-based surfaces with unmodified particles (Figure 8B) were used.

All particle-based surfaces accumulated higher amounts of bacteria than the respective flat control (Figure 8A). However, an effect of the particle size could be demonstrated. Regardless of the polymer shell, the lowest amounts of bacteria were always detected on surfaces based on 100 nm particles, suggesting that low surface roughness reduces bacterial adherence. Within the 100 nm particle coatings group, roughness-dependent differences can also be observed, as most bacteria were detected on P(SBMA-3) surfaces, which have the highest surface roughness (Figure 8). Notably, bacterial adhesion on 100 nm-SiO_2-P(CBMA-2) surfaces could not be quantified as these surfaces have a high intrinsic fluorescence, making analysis impossible (Figure S10, Supporting Information). With increasing particle size, significantly more bacteria accumulated on the particle-based surfaces (Figure 8A and Figures S11 and S12, Supporting Information), where a difference between the 400 nm and the 800 nm coatings could only be detected for SiO_2-P(MPC-2) based surfaces. Surfaces based on 400 nm SiO_2-P(MPC-2) modified particles reduced bacterial adhesion even more effectively than the corresponding SiO_2-P(EGMA) control. It can be generally concluded that the roughness of the surfaces significantly

**ADVANCED
SCIENCE NEWS**

www.advancedsciencenews.com

acro-
molecular
Chemistry and Physics

www.mcp-journal.de

influences their adhesion properties, with smoother surfaces (Rq < 100 nm) showing better anti-adhesion properties. This finding has already been made in several publications.[31–33] However, other surface parameters also appear to influence bacterial adhesion. For example, 400 nm SiO_2-P(SBMA-3) and 400 nm SiO_2-P(MPC-2) surfaces with almost the same surface roughness (Figure 8) showed significantly different bacterial adhesion. To illustrate this effect, the bacterial adhesion data of the particle-based, polymer-functionalized surfaces were compared with conditions in which the particles are non-functionalized (Figure 8B). For all tested coatings (except for coatings based on 800 nm SiO_2-P(MPC-2) particles), a significant effect of the polymer coating could be demonstrated. This effect was most pronounced for coatings based on 100 nm particles and decreased gradually with increasing particle size. While all coatings based on the zwitterionic polymers (except for P(CBMA-2) for the reasons mentioned) show similarly low bacterial colonization as P(EGMA) for coatings based on 100 nm particles, only P(MPC-2) reaches this level for coatings based on 400 nm particles. For coatings based on 800 nm particles, all zwitterionic coatings show higher bacterial colonization than the P(EGMA) control.

3. Conclusion

In this work, we report on the design and characterization of planar surfaces of zwitterionic polymer brushes as well as microstructured surfaces based on core-shell particles derived from these polymer brushes. For this, zwitterionic polymer brushes based on poly(sulfobetaines), poly(carboxybetaines), and poly(phosphorylcholines) are synthesized and used as potential antifouling coatings compared with the gold standard polymer P(EGMA).

First, zwitterionic brushes were synthesized on flat silicon substrates. Ellipsometry, AFM imaging, force-distance measurements, contact angle, and zeta potential measurements revealed thickness, topography and swelling, wettability, and acid-base properties of the brush-covered surfaces and verified the success of the grafting. Bacterial settlement on these substrates was investigated and it was found that zwitterionic polymer brushes have similar antifouling properties as P(EGMA) coatings. Since polymer brushes are known to lack stability and scalability on flat surfaces, core-shell particles of silica spheres with different diameters and zwitterionic polymer shells were synthesized. Electrokinetic measurements showed the influence of the zwitterionic shells on the zeta potential of the particles over a broad pH range (pH 2.5–10). These particles were processed by drop-casting into dense particle coatings whose topography and roughness were characterized by AFM and SEM.

The bacteria settlement of gram-negative *E. coli* bacteria on these coatings was subsequently investigated. It was found that bacterial adhesion increases with particle diameter and thus with the roughness of the zwitterionic coating. Moreover, the lower the roughness of the coating, the more pronounced the influence of the chemical composition of the surface on the adhesion of the bacteria. In particular, highly swollen coatings based on poly(phosphorylcholine) P(MPC-2) coated particles (100 nm), which had low absolute zeta potential values, showed the lowest *E. coli* adhesion. Our results open up new possibilities for the substitution of 2D anti-fouling systems, which can only be pro-

Table 3. Layer model used for the calculation of the layer thickness.

Layer-Nr.	Layer	Refractive index n	Extinction coefficient k [L mol^{-1} cm^{-1}]
1	Si	3.8858	−0.0180
2	SiO_2	3.8858	0
3	APS + Br-In.	1.422	0
4	Polymer	1.5	0
5	Air	1	0

duced on a laboratory scale, with large-area anti-fouling coatings based on particles with a diameter of 100 nm.

4. Experimental Section

All chemicals were purchased from Sigma Aldrich (Darmstadt, Germany) in analytical grade if not stated otherwise: tetraethylorthosilicate (TEOS, Fluka, 99%), ammonia solution (NH_4OH, Acros, 28–30% solution), hydrogen peroxide (H_2O_2, VWR, 30%), ethanol abs. (EtOH, VWR, 99.9%), APTES (ABCR, 97%), α-bromoisobutyryl bromide (BrIn, 98%), propionyl bromide (97%), anhydrous dichloromethane (Fluka), triethylamine (Fluka), copper(II) bromide ($CuBr_2$, 99.999%), tin(II) 2-ethylhexanoate (95%), tris(2-pyridylmethyl)amine (TPMA, 98%), N,N,N′,N″,N″-pentamethyldiethylenetriamine (99%), ethyl α-bromoisobutyrate (EBiB, 98%), dichloromethane (Acros, 99.99%), 2-(dimethylamino)ethyl methacrylate (DMAEMA, 98%) was passed before polymerization through basic, neutral, and acidic aluminum oxides. The water was ultrapure and obtained using a Merck Millipore system (Billerica, MA, United States, conductivity: 0.055 µS cm^{-1}).

Synthesis of Cbma-2 Monomer: The synthesis of the carboxybetaine methacrylate (CBMA-2) monomer followed the procedure by Zhang et al.[9] To control the final product, ^{1}H-NMR was used (Figure S13, Supporting Information).

Pre-Modification and Surface-Initiated ATRP on Flat Model Systems: Polished single-crystal silicon wafers (<100>) (Si-Mat Silicon Materials, Landsberg, Germany) were used as flat model substrates. The silicon wafers were cleaned using an alkaline RCA solution (H_2O_2/H_2O/NH_4OH, ratio 1:1:1) for 1 h at 70°C. The thickness of the resulting uniform SiO_2 layer was measured by null-ellipsometry. SiO_2 pre-modification steps: 1) 3-aminopropyltriethoxysilan (APTES) treatment to introduce amino groups, and 2) attachment of the ATRP-initiator α-bromoisobutyryl bromide were performed as previously described.[10] The ATRP-initiator-modified wafers were placed in a test tube with a stirring bar. The monomer was dissolved in the associated solvent (Table S2, Supporting Information) and added to the test tube. $CuBr_2$ (0.025 M in MeOH), the ligand 2,2′-bipyridine (bpy; 0.05 M in MeOH), and EBiB (0.15 µL) were added to the test tube. The test tube was sealed with a septum and purged with argon using a gas balloon for 10 min. Then, the reducing agent (ascorbic acid; 0.1 M or 1 M in H_2O) was added and the gas balloon was removed. Polymerization parameters are listed in Table S2, Supporting Information. After the reaction time, the wafers were washed with a related solvent.

Null-Ellipsometry: The dry brush thickness of all coatings on the flat model systems was measured by a null-ellipsometer (OPTREL MULTI-SCOPE LASER Null-Ellipsometer, Berlin) with an integrated He-Ne laser ($\lambda = 632.8$ nm) and an angle of incidence of 70°. The ellipsometric angles Δ and Ψ were determined with an accuracy of ±0.001°. The associated software determined the layer thickness from the ellipsometric angles according to a layer model (**Table 3**).

Synthesis and modification of silica-based core-shell particles: Monodisperse silica particles (100–800 nm) were synthesized using a multistep sol-gel reaction based on the Stöber approach.[34,35]

To form 100 nm native SiO_2 particles, Tetraethyl orthosilicate (TEOS) was added dropwise to a mixture of absolute ethanol and ammonium

hydroxide (NH_4OH, 28–30%) and stirred (500 rpm) overnight at room temperature. These 100 nm SiO_2 particles can be used as starting material for synthesizing SiO_2 particles with a diameter of 200 nm. This procedure was repeated to produce 400 nm and 800 nm SiO_2 particles by using the previously produced particles as starting material for the following particle size until the desired diameter was achieved (see Table S2, Supporting Information). The particles were repeatedly washed with ethanol p.a., separated from the solvent, and dried in a vacuum at 60°C.[19]

To introduce amino groups to the particle surface (SiO_2-NH_2), the particles were then ground, dispersed in a 5% APTES solution, and stirred at 500 rpm at room temperature for 24 h. The modified particles were purified by multiple centrifugation steps in ethanol and dried at 60°C in a vacuum. The amino-functionalized particles were dispersed in anhydrous dichloromethane (DCM), and the ATRP initiator α-bromoisobutyryl bromide (Br-initiator) and triethylamine were added. The dispersion was stirred for 2 h at room temperature. Afterward, the SiO_2-BrIn particles were separated and cleaned with DCM and Ethanol by centrifugation and dried under reduced pressure at room temperature.

Atomic Force Microscopy (AFM): AFM measurements were performed using a Dimension ICON AFM (Bruker Corp.). Images in dry state were recorded in Soft Tapping Mode using Multi 75G-Al cantilevers (Budget Sensors, BG) with a resonant frequency of 60–90 kHz and a tip radius of < 10 nm. Measurements in solutions were performed in PeakForce Tapping mode with ScanAsyst fluid cantilevers (Bruker Corp.). Images in solutions were taken at different loads (0.5, 1, and 2 nN).

Force-distance curves were recorded as described in detail by Drechsler et al.[36] using the force constant of the cantilever given by the manufacturer and the cantilever sensitivity determined on uncoated areas of the Si wafers. To adjust the offset of the force-distance curves, a scratch was applied to the brushes, and its depth was determined from AFM images taken at different loads (0.5, 1, and 2 nN). Finally, the force-distance curves were shifted parallel to the x-axis to match the values obtained in this way (see crosses in the force-distance curves in Figure 2C).

From the AFM images, the RMS roughness and the developed interfacial area ratio (Sdr) were calculated for representative areas corresponding to $\approx$20 $\times$ 20 times the particle diameter using the NanoScope Analysis 1.9 software (Bruker Corp.).

Electrokinetic Measurements: The zeta potential of flat surfaces was determined by streaming current measurements using a SurPASS 3 (Anton Paar Gmbh, Austria) with an adjustable gap cell. Two wafer specimens (1 $\times$ 2 cm) were adjusted face-to-face with a slit height of 100–110 μm. The measuring liquid (1 mM KCl solution) was streamed through this slit. From the slope of the streaming potential versus pressure difference the zeta potential was calculated. The zeta potential of the bare and coated silica particles was determined by electrophoresis with a Zetasizer Nano ZS (Malvern Instruments Ltd.) equipped with an MPT-2 auto titrator. The particles were suspended with a concentration of 0.42 mg ml^{-1} in a 1 mM KCl solution. Both types of measurements were started at pH 5–6. Then the pH value was increased or decreased stepwise by titrating the measuring solution with either a 0.1 M KOH or a 0.1 M HCl solution. The zeta potential was determined in triplicate at each adjusted pH value.

Dynamic Light Scattering (DLS): The size of the particles was determined using a Zetasizer Nano ZS (Malvern Instruments Ltd.) with an integrated laser (λ = 633 nm). Particles dispersed in an aqueous 10^{-3} M KCl solution were measured at 24°C unless otherwise described.

Scanning Electron Microscopy (SEM): For scanning electron microscopy (SEM) images, the samples were coated with 3.5 nm platinum to enhance the electron density using a Leica EM SCD500 sputter coater and imaged with a NEON 40 EsB CrossBeam scanning electron microscope (Carl Zeiss NTS GmbH, Germany). The sample was irradiated with a 3 keV electron beam in secondary electron mode.

Thermogravimetric Analysis (TGA): Thermogravimetric analysis (TGA) was carried out to calculate the polymer ratio of the core-shell particles. All measurements were performed in a nitrogen atmosphere on a TGA Q 5000IR analyzer (TA Instruments, USA).

Quartz Crystal Microbalance (QCM): QCM measurements were performed using a QCM-D model E4 (Biolin Scientific) equipped with a peristaltic pump system (IPC, Ismatec). Gold-coated quartz crystals (QSX301,

Quantum Design) with a resonance frequency of 5 MHz were used as substrates. Polymer coatings were prepared on the QCM crystals as described previously. All measurements were performed at a flow rate of 100 μL•min^{-1}. Protein solution (bovine serum albumin and fibrinogen [100 μg protein per mL PBS]) in PBS was adsorbed to the samples for 1 h and subsequently subjected to a desorption regime for 30 min with PBS. Frequency and dissipation shifts induced by the adsorbed proteins were recorded in real-time at the 3rd, 5th, 7th, 9th, 11th, and 13th overtones (15, 25, 35, 45, 55, and 65 MHz, respectively). The mass of adsorbed protein was calculated using the Sauerbrey equation[31] with the Q-Sense D Find software (Biolin Scientific).

Bacterial Adhesion Assay: GFP expressing *E. coli* (strain W3110) were grown overnight from a single colony in lysogenic broth (LB) at 30°C and 200 rpm. The next day, the overnight culture was diluted 1:100 in fresh LB and grown to an OD600 of 0.2, and the sample substrates were incubated in the bacterial solution at 37°C (without shaking) for 1 h. After incubation, adherent bacteria were fixed with 4% glutaraldehyde in phosphate-buffered saline for 10 min, washed in fresh PBS and Milli-Q water, and dried under nitrogen. Samples were imaged using confocal microscopy (SP5, Leica Microsystems) with a 10× objective (Figures S7 and S9, Supporting Information). For each sample, at least six images were acquired at random positions, and adherent cells were quantified with Fiji by determining the area occupied by the GFP signal concerning the total area of the image. The determined cell occupancy was normalized against the average value of the silicon reference in the respective experiment for the relative comparison between different experiments.

Supporting Information

Supporting Information is available from the Wiley Online Library or from the author.

Conflict of Interest

The authors declare no conflict of interest.

Author Contributions

A.S. and J.F. conceived the idea and designed the experiments. F.K, A.D., M.P., A.C., and J.F. performed the experiments and data analysis. F.K., A.D., A.C., and S.L. wrote the manuscript. J.F., A.M., and A.S. revised the manuscript.

Data Availability Statement

The data that support the findings of this study are available from the corresponding author upon reasonable request.

[1] O. P. Abioye, C. A. Loto, O. S. I. Fayomi, *J. Bio- Tribo-Corros.* **2019**, *5*, 22.

[2] A. B. Asha, Y. Chen, H. Zhang, S. Ghaemi, K. Ishihara, Y. Liu, R. Narain, *Langmuir* **2019**, *35*, 1621.

[3] H. Chen, C. Zhao, M. Zhang, Q. Chen, J. Ma, J. Zheng, *Langmuir* **2016**, *32*, 3315.

[4] J. Baggerman, M. M. J. Smulders, H. Zuilhof, *Langmuir* **2019**, *35*, 1072.

[5] K. L. Prime, G. M. Whitesides, *J. Am. Chem. Soc.* **1993**, *115*, 10714.

[6] C.-M. Xing, F.-N. Meng, M. Quan, K. Ding, Y. Dang, Y.-K. Gong, *Acta Biomater.* **2017**, *59*, 129.

[7] W. Yandi, S. Mieszkin, P. Martin-Tanchereau, M. E. Callow, J. A. Callow, L. Tyson, B. Liedberg, T. Ederth, *ACS Appl. Mater. Interfaces.* **2014**, *6*, 11448.

[8] O. A. Mkhatresh, F. Heatley, *Polym. Int.* **2004**, *53*, 1336.

[9] Y. Zhang, Y. Liu, B. Ren, D. Zhang, S. Xie, Y. Chang, J. Yang, J. Wu, L. Xu, J. Zheng, *J. Phys. D: Appl. Phys.* **2019**, *52*, 403001.

[10] C. Marschelke, I. Raguzin, A. Matura, A. Fery, A. Synytska, *Soft Matter* **2017**, *13*, 1074.

[11] B. R. Knowles, D. Yang, P. Wagner, S. Maclaughlin, M. J. Higgins, P. J. Molino, *Langmuir* **2019**, *35*, 1335.

[12] K. Ishihara, N. P. Ziats, B. P. Tierney, N. Nakabayashi, J. M. Anderson, *J. Biomed. Mater. Res.* **1991**, *25*, 1397.

[13] E. Schönemann, A. Laschewsky, E. Wischerhoff, J. Koc, A. Rosenhahn, *Polymers* **2019**, *11*, 1014.

[14] H. Kang, W. Jeong, D. Hong, *Langmuir* **2019**, *35*, 7744.

[15] Y.-K. Gong, L. -P. Liu, P. B. Messersmith, *Macromol. Biosci.* **2012**, *12*, 979.

[16] B. R. Knowles, P. Wagner, S. Maclaughlin, M. J. Higgins, P. J. Molino, *Biointerphases* **2020**, *15*, 011001.

[17] J. Li, D. Tan, X. Zhang, H. Tan, M. Ding, C. Wan, Q. Fu, *Colloids Surf., B* **2010**, *78*, 343.

[18] J.-S. Wang, K. Matyjaszewski, *J. Am. Chem. Soc.* **1995**, *117*, 5614.

[19] C.-J. Lee, H. Wu, Q. Tang, B. Cao, H. Wang, H. Cong, J. Zhe, F. Xu, G. Cheng, *Langmuir* **2015**, *31*, 9965.

[20] M. Veiseh, M. H. Zareie, M. Zhang, *Langmuir* **2002**, *18*, 6671.

[21] M. Ezzat, C.-J. Huang, *RSC Adv.* **2016**, *6*, 61695.

[22] M. Kobayashi, M. Terada, A. Takahara, *Faraday Discuss.* **2012**, *156*, 403.

[23] X. Sun, H. Wang, Y. Wang, T. Gui, K. Wang, C. Gao, *Biosens. Bioelectron.* **2018**, *102*, 63.

[24] A. Synytska, E. Biehlig, L. Ionov, *Macromolecules* **2014**, *47*, 8377.

[25] D. Nagasawa, T. Azuma, H. Noguchi, K. Uosaki, M. Takai, *J. Phys. Chem. C.* **2015**, *119*, 17193.

[26] S. Berger, A. Synytska, L. Ionov, K.-J. Eichhorn, M. Stamm, *Macromolecules* **2008**, *41*, 9669.

[27] M. Schwarzer, T. Otto, M. Schremb, C. Marschelke, H. T. Tee, F. R. Wurm, I. V. Roisman, C. Tropea, A. Synytska, *Chem. Mater.* **2019**, *31*, 112.

[28] S. Guo, D. Janczewski, X. Zhu, R. Quintana, T. He, K. G. Neoh, *J. Colloid Interface Sci.* **2015**, *452*, 43.

[29] T. Azuma, T. Matsushita, V. A. Manivel, K. Nilsson Ekdahl, B.o Nilsson, Y. Teramura, M. Takai, *J Biomater.* **2020**, *31*, 679.

[30] F. Hu, K. Chen, H. Xu, H. Gu, *Colloids Surf., B.* **2015**, *126*, 251.

[31] R. L. Taylor, J. Verran, G. C. Lees, A. J. P. Ward, *J. Mater. Sci.: Mater. Med.* **1998**, *9*, 17.

[32] C. H. F. Pereira Da Silva, G. M. Vidigal, M. De Uzeda, G. De Almeida Soares, *Implant Dent.* **2005**, *14*, 88.

[33] A. Braem, L. Van Mellaert, D. Hofmans, E. De Waelheyns, J. Anné, J. Schrooten, J. Vleugels, *Powder Metall.* **2013**, *56*, 267.

[34] W. Stöber, A. Fink, E. Bohn, *J. Colloid Interface Sci.* **1968**, *26*, 62.

[35] K. Nozawa, H. Gailhanou, L. Raison, P. Panizza, H. Ushiki, E. Sellier, J. P. Delville, M. H. Delville, *Langmuir* **2005**, *21*, 1516.

[36] A. Drechsler, A. Synytska, P. Uhlmann, M. M. Elmahdy, M. Stamm, F. Kremer, *Langmuir* **2010**, *26*, 6400.